

Intrinsic piezoelectric ferromagnetism with large out-of-plane piezoelectric response in Janus monolayer $\text{CrBr}_{1.5}\text{I}_{1.5}$

San-Dong Guo¹, Xiao-Shu Guo¹, Xiu-Xia Cai¹, Wen-Qi Mu¹ and Wen-Cai Ren^{2,3}

¹*School of Electronic Engineering, Xi'an University of Posts and Telecommunications, Xi'an 710121, China*

²*Shenyang National Laboratory for Materials Science, Institute of Metal Research, Chinese Academy of Science, 110016 Shenyang, Liaoning, P. R. China and*

³*School of Materials Science and Engineering, University of Science and Technology of China, Shenyang 110016, P. R. China*

A two-dimensional (2D) material system with both piezoelectricity and ferromagnetic (FM) order, referred to as a 2D piezoelectric ferromagnetism (PFM), may open up unprecedented opportunities for intriguing physics. Inspired by experimentally synthesized Janus monolayer MoSSe from MoS₂, in this work, the Janus monolayer $\text{CrBr}_{1.5}\text{I}_{1.5}$ with dynamic, mechanical and thermal stabilities is predicted, which is constructed from synthesized ferromagnetic CrI₃ monolayer by replacing the top I atomic layer with Br atoms. Calculated results show that monolayer $\text{CrBr}_{1.5}\text{I}_{1.5}$ is an intrinsic FM half semiconductor with valence and conduction bands being fully spin-polarized in the same spin direction. Furthermore, monolayer $\text{CrBr}_{1.5}\text{I}_{1.5}$ possesses a sizable magnetic anisotropy energy (MAE). By symmetry analysis, it is found that both in-plane and out-of-plane piezoelectric polarizations can be induced by a uniaxial strain in the basal plane. The calculated in-plane d_{22} value of 0.557 pm/V is small. However, more excitingly, the out-of-plane d_{31} is as high as 1.138 pm/V, which is obviously higher compared with ones of other 2D known materials. The strong out-of-plane piezoelectricity is highly desirable for ultrathin piezoelectric devices. Moreover, strain engineering is used to tune piezoelectricity of monolayer $\text{CrBr}_{1.5}\text{I}_{1.5}$. It is found that compressive strain can improve the d_{22} , and tensile strain can enhance the d_{31} . A FM order to antiferromagnetic (AFM) order phase transition can be induced by compressive strain, and the critical point is about 0.95 strain. That is to say that a 2D piezoelectric antiferromagnetism (PAFM) can be achieved by compressive strain, and the corresponding d_{22} and d_{31} are 0.677 pm/V and 0.999 pm/V at 0.94 strain, respectively. It is also found that magnetic order has important effects on piezoelectricity of monolayer $\text{CrBr}_{1.5}\text{I}_{1.5}$. Finally, similar to $\text{CrBr}_{1.5}\text{I}_{1.5}$, the PFM can also be realized in the monolayer $\text{CrF}_{1.5}\text{I}_{1.5}$ and $\text{CrCl}_{1.5}\text{I}_{1.5}$. Amazingly, their d_{31} can reach up to 2.578 pm/V and 1.804 pm/V for monolayer $\text{CrF}_{1.5}\text{I}_{1.5}$ and $\text{CrCl}_{1.5}\text{I}_{1.5}$. Our works propose a realistic way to achieve PFM with large d_{31} , making these systems very promising for multifunctional semiconductor spintronic applications.

PACS numbers: 71.20.-b, 77.65.-j, 72.15.Jf, 78.67.-n

Email:sandongyuwang@163.com

Keywords: Ferromagnetism, Piezoelectronics, 2D materials

I. INTRODUCTION

The piezoelectric effect is an intrinsic electromechanical coupling in semiconductors with crystal structures lacking inversion symmetry. The reduction in dimensionality of 2D materials often can eliminate inversion symmetry, which allows them to be piezoelectric. Experimentally, the piezoelectricity of MoS₂^{1,2}, MoSSe³ and In₂Se₃⁴ monolayers have been discovered, which pushes the development of piezoelectric properties of 2D materials. In theory, many kinds of 2D materials have been predicted to be piezoelectric by density functional theory (DFT) calculations^{5–12}. The strain-tuned piezoelectric response has also been investigated by DFT calculations, and it is proved that strain can improve the piezoelectric strain coefficients^{13–15}.

Great advances have been made on 2D piezoelectric materials. However, there are two main issues of 2D piezoelectric materials. One is that most 2D materials possess solely piezoelectricity. The multifunctional 2D materials, such as combination of piezoelectricity with topological insulating phase or ferromagnetism, are of particular interest, whose exploitation may promise novel device applications. The coexistence of intrinsic piezo-

electricity and ferromagnetism has been predicted in 2D vanadium dichalcogenides and VSi₂P₄^{16,17}. The piezoelectric quantum spin Hall insulators (PQSHI) have also been achieved in monolayer InXO (X=Se and Te)¹⁸ and Janus monolayer SrAlGaSe₄¹⁹. Another is that the out-of-plane piezoelectricity in known 2D materials is absent or weak. The strong out-of-plane piezoelectric effect and its inverse effect are highly desirable for piezoelectric devices, which is compatible with the bottom/top gate technologies. Many strategies have been made for searching 2D piezoelectric materials with large d_{31} or d_{32} ^{5,11,20–22}. A significant improvement is that the piezoelectric strain coefficient d_{31} of Sc₂CO₂ MXene is up to 0.78 pm/V²².

A natural idea is to search for multifunctional 2D piezoelectric materials with large out-of-plane piezoelectricity. A few types of 2D magnetic materials have been studied^{23–31}. For example, the monolayer Cr₂Ge₂Te₆, VS₂ and VSe₂ have been experimentally proved to magnetic materials^{25,28}. The Dirac spin-gapless semiconductor (SGS) with 100% spin polarization, high Fermi velocities and high Curie temperatures has been predicted in Mn₂C₆Se₁₂ and Mn₂C₆S₆Se₆ monolayers²⁹. The 2D high-temperature ferromagnetic half-metal (FMHM) can be realized in transition-metal embedded carbon nitride

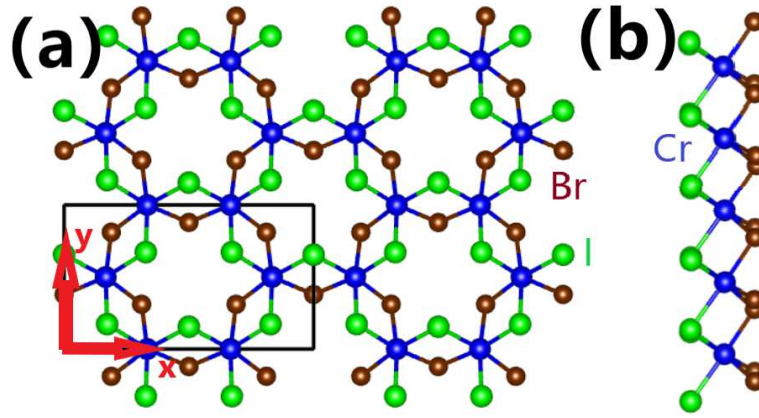


FIG. 1. (Color online) The (a) top view and (b) side view of crystal structure of Janus monolayer $\text{CrBr}_{1.5}\text{I}_{1.5}$. The rectangle supercell is marked by black frame, which is used to calculate the piezoelectric stress coefficients. The rectangle's width and height are defined as x and y directions, respectively.

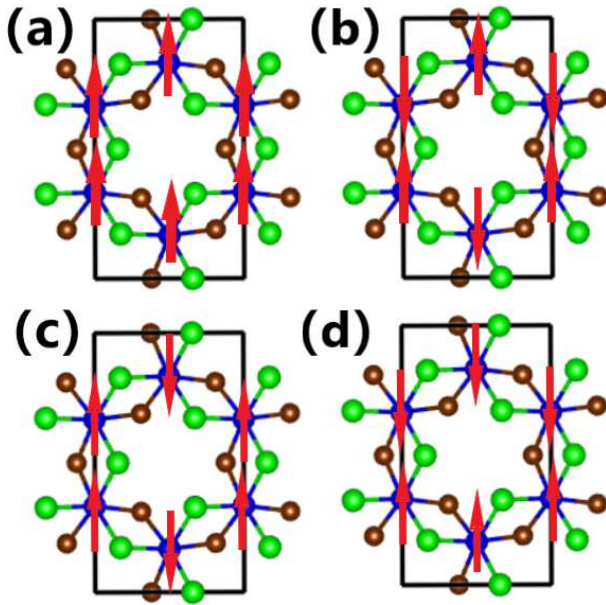


FIG. 2. (Color online) The four considered magnetic configuration of Janus monolayer $\text{CrBr}_{1.5}\text{I}_{1.5}$: FM (a), AF-Néel (b), AF-zigzag (c), and AF-stripy ordered (d). The crystal cells used in the calculations are marked with red arrows as the spin direction of Cr atoms.

monolayers²⁷. The CrI_3 monolayer is firstly predicted to be FM order by the first-principle calculations³², and then is confirmed experimentally³⁰. A series of studies have been carried out to explore the magnetic related properties in CrI_3 monolayer³³⁻³⁸. These provide many new possibilities to combine the piezoelectricity and magnetism into the same kind of 2D material.

It is noted that the CrI_3 monolayer has sandwiched I-Cr-I structure with inversion symmetry, and then possesses no piezoelectricity. However, it is possible to construct Janus structure based on CrI_3 monolayer, and then produce piezoelectric effect. Janus monolayer MoSSe has

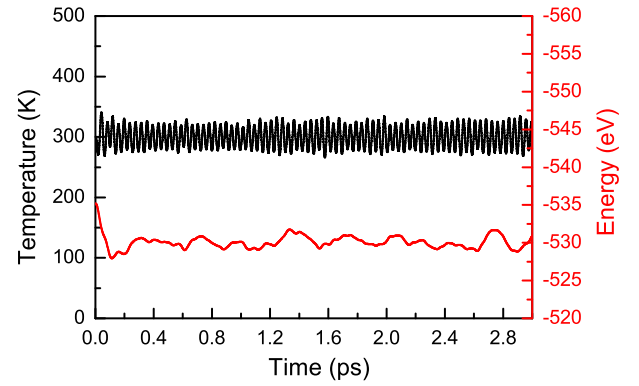


FIG. 3. (Color online) The temperature and total energy fluctuations of Janus monolayer $\text{CrBr}_{1.5}\text{I}_{1.5}$ with FM magnetic configuration at 300 K.

been synthesized experimentally from MoS_2 monolayer by breaking the out-of-plane structural symmetry³⁹. That is, the Janus monolayer MoSSe can be constructed by replacing one of two S layers with Se atoms in MoS_2 monolayer. In this work, Janus monolayer $\text{CrBr}_{1.5}\text{I}_{1.5}$ is constructed from synthesized ferromagnetic CrI_3 monolayer by replacing the top I atomic layer with Br atoms, which is dynamically, mechanically and thermally stable. It is found that monolayer $\text{CrBr}_{1.5}\text{I}_{1.5}$ is an intrinsic FM half semiconductor with a sizable MAE. Although the calculated in-plane d_{22} (0.557 pm/V) is small, the out-of-plane d_{31} (1.138 pm/V) is very large, which is obviously higher than ones of other 2D known materials. It is proved that strain engineering can effectively tune piezoelectricity of monolayer $\text{CrBr}_{1.5}\text{I}_{1.5}$. A 2D PAFM can also be achieved in monolayer $\text{CrBr}_{1.5}\text{I}_{1.5}$ by compressive strain, and the calculated results show that magnetic order has important influences on piezoelectricity of monolayer $\text{CrBr}_{1.5}\text{I}_{1.5}$. It is also proved that the PFM can also be achieved in monolayer $\text{CrF}_{1.5}\text{I}_{1.5}$ and monolayer $\text{CrCl}_{1.5}\text{I}_{1.5}$, which show very large d_{31} of 2.578 pm/V and

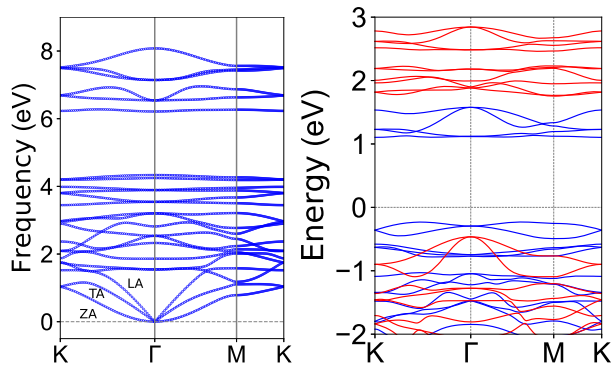


FIG. 4. (Color online) Left: the phonon band dispersions of Janus monolayer $\text{CrBr}_{1.5}\text{I}_{1.5}$ with FM magnetic configuration. Right: the energy band structures of $\text{CrBr}_{1.5}\text{I}_{1.5}$ with FM state. The blue (red) lines represent the band structure in the spin-up (spin-down) direction.

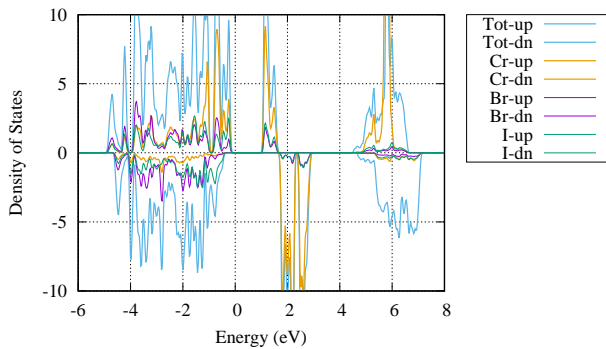


FIG. 5. (Color online) Calculated total and atomic partial density of states of Janus monolayer $\text{CrBr}_{1.5}\text{I}_{1.5}$ with FM magnetic configuration.

1.804 pm/V.

The rest of the paper is organized as follows. In the next section, we shall give our computational details and methods. In the next few sections, we shall present structural stabilities, electronic structures, and piezoelectric properties of monolayer $\text{CrBr}_{1.5}\text{I}_{1.5}$, along with strain effects on its piezoelectric properties. Finally, we shall give our discussion and conclusions.

II. COMPUTATIONAL DETAIL

Within DFT⁴⁰, we perform the main calculations with spin-polarization using the the plane-wave code VASP^{41–43} within the projector augmented-wave (PAW) method. The popular generalized gradient approximation of Perdew, Burke and Ernzerhof (GGA-PBE)⁴⁴ is used as the exchange-correlation functional. The kinetic energy cutoff is set to 500 eV with the total energy convergence criterion for 10^{-8} eV. All the lattice constants and atomic coordinates are optimized until the force on each atom is less than $0.0001 \text{ eV} \cdot \text{Å}^{-1}$. A vacuum spacing

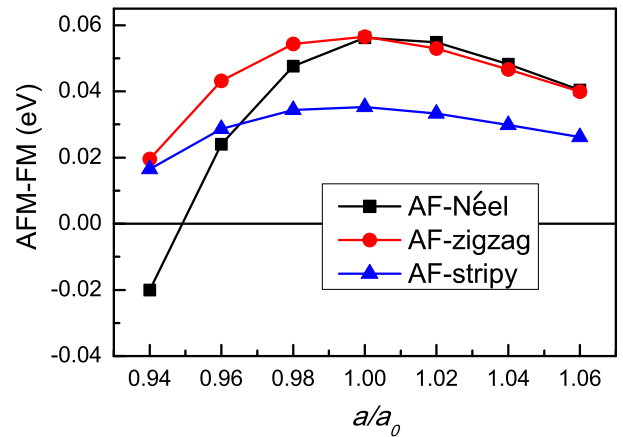


FIG. 6. (Color online) Calculated energy differences of AF-Néel, AF-zigzag and AF-stripy with respect to FM state as a function of strain with rectangle supercell.

of more than 18 Å is used to avoid interactions between two neighboring images. The elastic stiffness tensor C_{ij} and piezoelectric stress tensor e_{ij} are carried out by using strain-stress relationship (SSR) and density functional perturbation theory (DFPT) method⁴⁵, respectively. A Monkhorst-Pack k-mesh of $8 \times 8 \times 1$ is used to sample the Brillouin Zone (BZ) for the calculations of electronic structure and elastic coefficients C_{ij} , and a mesh of $4 \times 8 \times 1$ k-points for the energy of different magnetic configurations and piezoelectric stress coefficients e_{ij} . The 2D elastic coefficients C_{ij}^{2D} and piezoelectric stress coefficients e_{ij}^{2D} have been renormalized by $C_{ij}^{2D} = Lz C_{ij}^{3D}$ and $e_{ij}^{2D} = Lz e_{ij}^{3D}$, where the Lz is the length of unit cell along z direction. By finite displacement method, the interatomic force constants (IFCs) are obtained based on the $4 \times 4 \times 1$ supercell with FM ground state. Based on the harmonic IFCs, the phonon dispersions are evaluated using Phonopy code⁴⁶.

III. STRUCTURE AND STABILITY

The structure of Janus monolayer $\text{CrBr}_{1.5}\text{I}_{1.5}$ is similar to monolayer CrI_3 monolayer, which contains three atomic sublayers with Cr layer sandwiched between Br and I layers. It is well known that Janus transition metal dichalcogenides (TMD) Monolayer MoSSe has been synthesized by replacing the top S atomic layer in MoS_2 with Se atoms³⁹. Using the same idea, the Janus monolayer $\text{CrBr}_{1.5}\text{I}_{1.5}$ can be constructed by replacing one of two I layers with Br atoms in monolayer CrI_3 . The schematic crystal structures of Janus monolayer $\text{CrBr}_{1.5}\text{I}_{1.5}$ are shown in Figure 1. The monolayer CrI_3 has centrosymmetry with $\bar{3}m$ point-group symmetry (No.162), but monolayer $\text{CrBr}_{1.5}\text{I}_{1.5}$ loses centrosymmetry and horizontal mirror symmetry with $3m$ point-group symmetry (No.157), which will induce both in-plane and out-of-plane piezoelectricity.

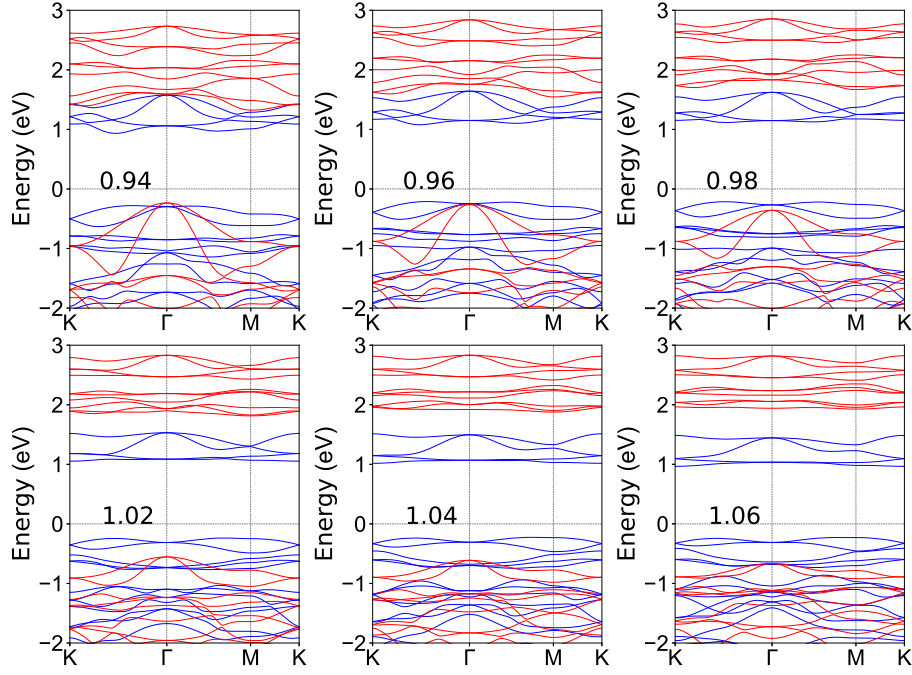


FIG. 7. (Color online) The energy band structures of Janus monolayer $\text{CrBr}_{1.5}\text{I}_{1.5}$ with FM magnetic configuration with a/a_0 changing from 0.94 to 1.06.

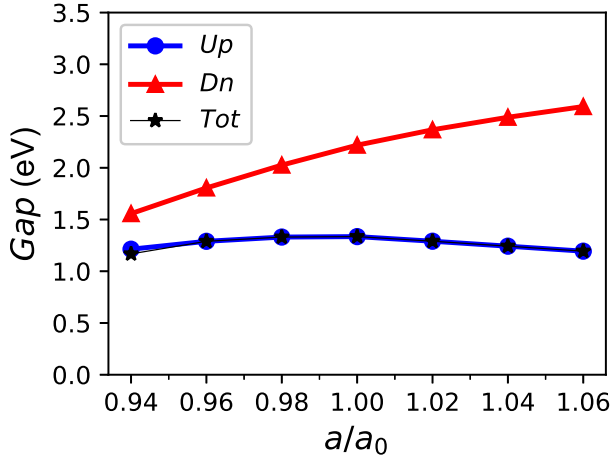


FIG. 8. (Color online) The majority-spin gap (Up), the minority-spin gap (Dn) and the total gap (Tot) of FM $\text{CrBr}_{1.5}\text{I}_{1.5}$ as a function of strain a/a_0 .

Four different magnetic configurations (Figure 2) are considered to evaluate the magnetic ground state of monolayer $\text{CrBr}_{1.5}\text{I}_{1.5}$, which are used to investigate the ground state of monolayer CrX_3 ($X=\text{F}, \text{Cl}, \text{Br}$ and I)³². The energy of AF-Néel, AF-zigzag, AF-stripy state and non-magnetic (NM) state with respect to FM state are 56.1 meV, 56.4 meV, 35.2 meV and 6.802 eV with rectangle supercell. Our calculated results show that the FM order is the most stable magnetic state. This means that ferromagnetism in monolayer CrI_3 is retained by elements substitution to construct Janus structure. The optimized

lattice constants with FM state is 6.744 Å, which falls between those of the CrBr_3 (6.433 Å) and CrI_3 (7.008 Å) monolayers³². For monolayer $\text{CrBr}_{1.5}\text{I}_{1.5}$, the difference in atomic sizes and electronegativities of Br and I atoms leads to inequivalent Cr-Br and Cr-I bond lengths (Br-Cr-Br and I-Cr-I bond angles), and they are 2.542 Å and 2.719 Å (92.036 and 89.432), which can induce a built-in electric field.

The ab initio molecular dynamics (AIMD) simulations using NVT ensemble are performed to assess the thermal stability of the monolayer $\text{CrBr}_{1.5}\text{I}_{1.5}$ at room temperature. Figure 3 shows the temperature and total energy fluctuations of $\text{CrBr}_{1.5}\text{I}_{1.5}$ monolayer as a function of the simulation time. Calculated results show no obvious structural disruption with the temperature and total energy fluctuates being small at the end of the MD simulation at 300 K, which confirms the thermodynamical stability of the $\text{CrBr}_{1.5}\text{I}_{1.5}$ monolayer at room temperature.

The dynamical stability of the $\text{CrBr}_{1.5}\text{I}_{1.5}$ monolayer is analyzed by the phonon spectra, which is plotted in Figure 4. There are twenty-one optical and three acoustical phonon branches with a total of twenty-four branches due to eight atoms per cell. The longitudinal acoustic (LA) and transverse acoustic (TA) modes mean in-plane vibrations, while the ZA branch represents the out-of-plane vibrations. It is clearly seen that the ZA branch is quadratic near the zone center, as typical characteristics of 2D materials^{47,48}. All phonon frequencies are positive, confirming the dynamical stability of $\text{CrBr}_{1.5}\text{I}_{1.5}$ monolayer, which means that it can exist as a free-standing

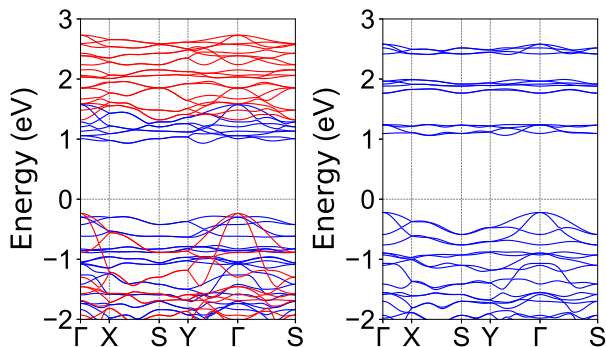


FIG. 9. (Color online) The energy band structures of $\text{CrBr}_{1.5}\text{I}_{1.5}$ with FM (Left) and AF-Néel (Right) states at 0.94 strain. The blue (red) lines represent the band structure in the spin-up (spin-down) direction.

2D crystal.

It is important to check the mechanical stability of $\text{CrBr}_{1.5}\text{I}_{1.5}$ monolayer for practical application. Therefore, we calculate elastic constants using the SSR method. Using Voigt notation, the elastic tensor with $\bar{3}m$ point-group symmetry for 2D materials can be expressed as:

$$C = \begin{pmatrix} C_{11} & C_{12} & 0 \\ C_{12} & C_{11} & 0 \\ 0 & 0 & (C_{11} - C_{12})/2 \end{pmatrix} \quad (1)$$

The calculated C_{11} and C_{12} are 29.75 Nm^{-1} and 8.26 Nm^{-1} , which are between ones of CrBr_3 and CrI_3 monolayers³². The calculated $C_{11} > 0$ and $C_{11} - C_{12} > 0$ satisfy the Born criteria of mechanical stability⁴⁹, confirming the mechanical stability of $\text{CrBr}_{1.5}\text{I}_{1.5}$ monolayer. We also calculate the Young's moduli C_{2D} , shear modulus G_{2D} and Poisson's ratio ν using the method suggested by Andrew et al, and they are 27.46 Nm^{-1} , 10.75 Nm^{-1} and 0.278, respectively. These indicate that monolayer $\text{CrBr}_{1.5}\text{I}_{1.5}$ can be easily tuned by strain, which is favorable for novel flexible piezotronics and nanoelectronics.

IV. ELECTRONIC STRUCTURE

To exhibit piezoelectricity, the monolayer $\text{CrBr}_{1.5}\text{I}_{1.5}$ not only should lack inversion symmetry, but also should be a semiconductor. So, we investigate the electronic structures of $\text{CrBr}_{1.5}\text{I}_{1.5}$ monolayer with FM ground state, and the energy bands and atomic partial density of states (DOS) are plotted in Figure 4 and Figure 5, respectively. It is found that $\text{CrBr}_{1.5}\text{I}_{1.5}$ monolayer is an indirect gap semiconductor with gap value of 1.335 eV. Moreover, the valence and conduction bands near the Fermi level are exclusively contributed by the same spin-up component, showing a typical half-semiconductor character. The difference of the band edge energy between the two spin components for the conduction band minimum (CBM) and the valence band maximum (VBM) are

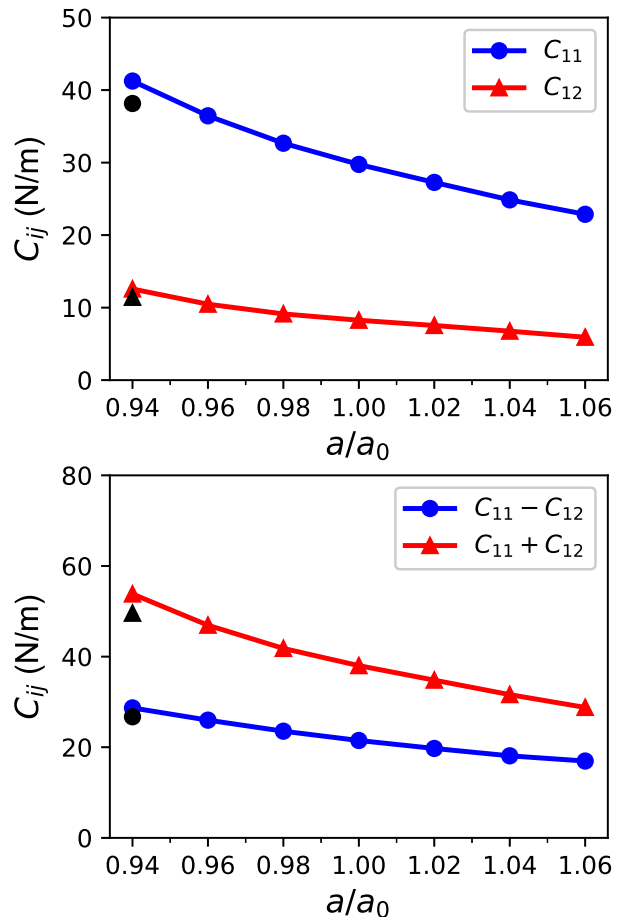


FIG. 10. (Color online) For Janus monolayer $\text{CrBr}_{1.5}\text{I}_{1.5}$ with FM state, the elastic constants C_{ij} with the application of biaxial strain (0.94 to 1.06). The black marks mean AF-Néel results at 0.94 strain.

0.884 eV and 0.233 eV, respectively. According to DOS, the occupied Cr-3d orbitals are mainly found in the spin-up direction, and the spin-down Cr-3d states are almost unoccupied. For both spin directions, the conduction band is dominated by Cr-3d states, which are weakly hybridized with the Br-3p and I-3p states. In the spin-down direction, the valence bands are almost pure Br-3p and I-3p character. For the spin-up direction of the valence band, the states are contributed by the Br-3p and I-3p states with a mixture of Cr-3d states. In fact, many electronic properties of monolayer $\text{CrBr}_{1.5}\text{I}_{1.5}$ are similar to ones of CrI_3 monolayer³².

The magnetic moment of primitive cell is equal to $6 \mu_B$ accurately, which is consistent with its semiconducting property. The local magnetic moments of Cr is 2.985 μ_B , which suggests that monolayer $\text{CrBr}_{1.5}\text{I}_{1.5}$ is robust intrinsic ferromagnetic 2D semiconductor with large magnetic moments. MAE is an important parameter to confirm ferromagnetic behavior of monolayer $\text{CrBr}_{1.5}\text{I}_{1.5}$. The small MAE will result in superparamagnetic rather than ferromagnetic behavior. By using GGA+spin orbital coupling (SOC), it is found that an easy axis is

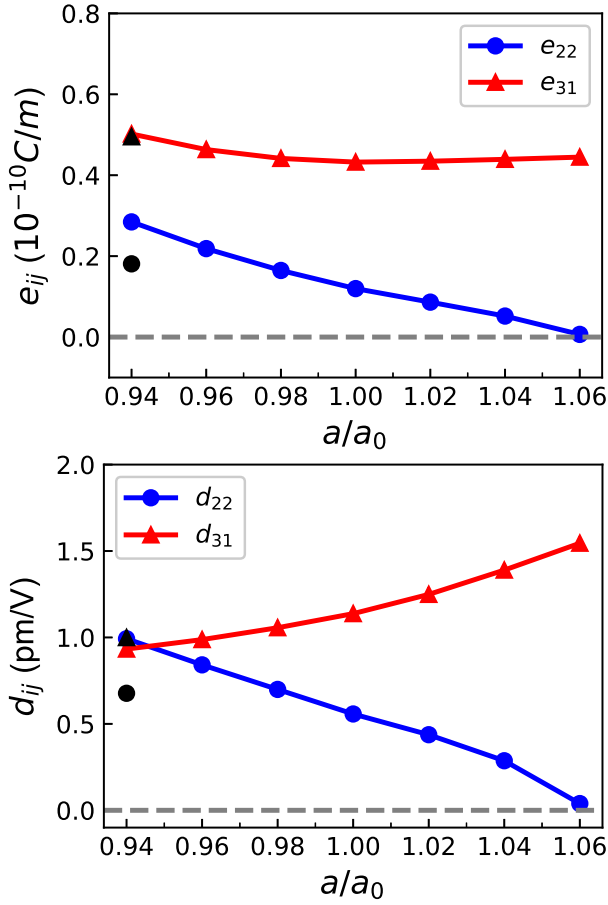


FIG. 11. (Color online) For Janus monolayer $\text{CrBr}_{1.5}\text{I}_{1.5}$ with FM state, the piezoelectric stress coefficients (e_{22} and e_{31}) and the piezoelectric strain coefficients (d_{22} and d_{31}) with the application of biaxial strain (0.94 to 1.06). The black marks mean AF-Néel results at 0.94 strain.

along the c -direction for monolayer $\text{CrBr}_{1.5}\text{I}_{1.5}$, and the corresponding MAE is $356 \mu\text{eV}$ per Cr atom. For CrBr_3 and CrI_3 monolayers, the easy axis is also along the c -direction, and the MAE of monolayer $\text{CrBr}_{1.5}\text{I}_{1.5}$ is between ones of them ($185.5 \mu\text{eV}$ per Cr atom for CrBr_3 and $685.5 \mu\text{eV}$ per Cr atom for CrI_3)³².

V. PIEZOELECTRIC PROPERTIES

The CrI_3 monolayer with $\bar{3}m$ point-group symmetry are centrosymmetric, showing no piezoelectricity. The $\text{CrBr}_{1.5}\text{I}_{1.5}$ monolayer with $3m$ point-group symmetry lacks both inversion symmetry and reflectional symmetry across the xy plane, which means that both e_{22}/d_{22} and e_{31}/d_{31} with defined x and y direction in Figure 1 are nonzero. For 2D materials, only the in-plane strain and stress are taken into account^{5–12}, and the piezoelectric stress and strain tensors by using Voigt notation can

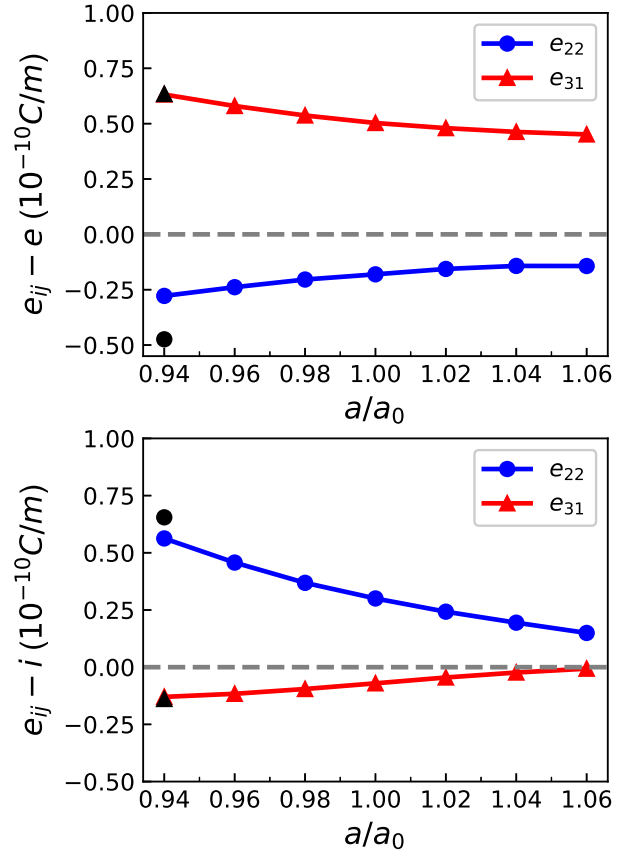


FIG. 12. (Color online) For Janus monolayer $\text{CrBr}_{1.5}\text{I}_{1.5}$ with FM state, the ionic contribution and electronic contribution to e_{22} and e_{31} with the application of biaxial strain (0.94 to 1.06). The black marks mean AF-Néel results at 0.94 strain.

become:

$$e = \begin{pmatrix} 0 & 0 & -e_{22} \\ -e_{22} & e_{22} & 0 \\ e_{31} & e_{31} & 0 \end{pmatrix} \quad (2)$$

$$d = \begin{pmatrix} 0 & 0 & -2d_{22} \\ -d_{22} & d_{22} & 0 \\ d_{31} & d_{31} & 0 \end{pmatrix} \quad (3)$$

With a applied uniaxial in-plane strain, both in-plane and vertical piezoelectric polarization ($e_{22}/d_{22} \neq 0$ and $e_{31}/d_{31} \neq 0$) can be produced. However, by imposing biaxial in-plane strain, the out-of-plane one still will remain, while the in-plane piezoelectric response will be suppressed ($e_{11}/d_{11} = 0$ and $e_{31}/d_{31} \neq 0$). The independent d_{22} and d_{31} are can be attained by $e_{ik} = d_{ij}C_{jk}$:

$$d_{22} = \frac{e_{22}}{C_{11} - C_{12}} \quad \text{and} \quad d_{31} = \frac{e_{31}}{C_{11} + C_{12}} \quad (4)$$

The orthorhombic supercell is used as the computational unit cell (in Figure 1) to calculate the

TABLE I. For $\text{CrX}_{1.5}\text{I}_{1.5}$ ($X=\text{F}$, Cl and Br) monolayers, the lattice constants a_0 (\AA), the elastic constants C_{ij} in Nm^{-1} , the piezoelectric stress coefficients e_{ij} in 10^{-10} C/m , the piezoelectric strain coefficients d_{ij} in pm/V , MAE in $\mu\text{eV/Cr}$ and easy axis (EA).

Name	a_0	C_{11}	C_{12}	e_{22}	e_{31}	d_{22}	d_{31}	MAE	EA
$\text{CrF}_{1.5}\text{I}_{1.5}$	6.250	49.97	16.34	1.339	1.710	3.983	2.578	2151	ab
$\text{CrCl}_{1.5}\text{I}_{1.5}$	6.590	34.88	9.94	0.238	0.809	0.956	1.804	110	c
$\text{CrBr}_{1.5}\text{I}_{1.5}$	6.744	29.75	8.26	0.119	0.432	0.557	1.138	356	c

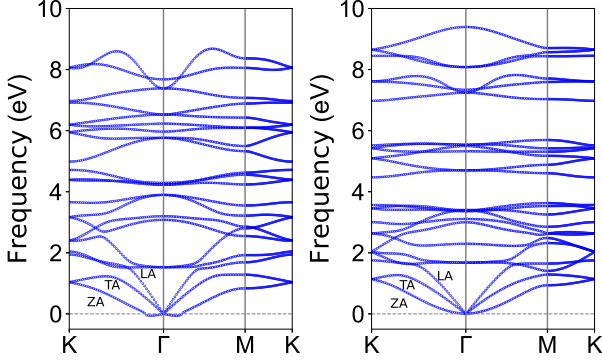


FIG. 13. (Color online) the phonon band dispersions of Janus monolayer $\text{CrF}_{1.5}\text{I}_{1.5}$ (Left) and $\text{CrCl}_{1.5}\text{I}_{1.5}$ (Right) with FM magnetic configuration.

e_{ij} of $\text{CrBr}_{1.5}\text{I}_{1.5}$ monolayer. The calculated e_{22} is 0.119×10^{-10} C/m with ionic part 0.300×10^{-10} C/m and electronic part -0.181×10^{-10} C/m , and e_{31} for 0.432×10^{-10} C/m with ionic contribution -0.071×10^{-10} C/m and electronic contribution 0.503×10^{-10} C/m . It is found that the electronic and ionic polarizations have opposite signs for both e_{22} and e_{31} . The ionic contribution to the in-plane piezoelectricity is larger than the electronic contribution. However, the electronic contributions dominate the out-of-plane piezoelectricity. Based on Equation 4, the d_{22} and d_{31} can be attained from previous calculated C_{ij} and e_{ij} . The calculated d_{22} and d_{31} are 0.557 pm/V and 1.138 pm/V . A large out-of-plane piezoelectric response is highly desired for 2D materials, which is compatible with the nowadays bottom/top gate technologies. The d_{31} of $\text{CrBr}_{1.5}\text{I}_{1.5}$ monolayer is obviously higher compared with ones of other 2D known materials, including the oxygen functionalized MXenes (0.40 - 0.78 pm/V)²², Janus TMD monolayers (0.03 pm/V)⁵, functionalized h-BN (0.13 pm/V)⁵⁰, kalium decorated graphene (0.3 pm/V)⁵¹, Janus group-III materials (0.46 pm/V)¹¹, Janus BiTeI/SbTeI monolayer (0.37 - 0.66 pm/V)⁵² and α - In_2Se_3 (0.415 pm/V)⁵³. To the best of our knowledge, the d_{31} is less than one among all pure 2D materials. So, it is very peculiar that the d_{31} of $\text{CrBr}_{1.5}\text{I}_{1.5}$ monolayer is as high as 1.138 pm/V .

VI. STRAIN EFFECTS

The strain can effectively tune the electronic structures and piezoelectric properties of 2D materials¹³⁻¹⁵. Here, we use a/a_0 to simulate the biaxial strain, where a and a_0 are the strained and unstrained lattice constants, respectively. To determine the ground state of strained $\text{CrF}_{1.5}\text{I}_{1.5}$ monolayer, four different initial magnetic configurations (Figure 2) are considered. The energy differences of AF-Néel, AF-zigzag and AF-stripy with respect to FM state as a function of strain with rectangle supercell are shown in Figure 6. It is found that a magnetic phase transition can be induced by compressive strain with the critical point being about 0.95 , which implies the robustness of the intrinsic ferromagnetism in $\text{CrF}_{1.5}\text{I}_{1.5}$ monolayer. Calculated results show that $\text{CrF}_{1.5}\text{I}_{1.5}$ monolayer prefers FM ground state with a/a_0 being greater than about 0.95 in considered strain range, and the AF-Néel become ground state with a/a_0 being less than about 0.95 . Similar phenomenon can also be found in CrI_3 monolayer, and the AF-Néel phase becomes the most stable phase at 0.92 strain³².

The energy band structures of FM $\text{CrF}_{1.5}\text{I}_{1.5}$ monolayer with strain from 0.94 to 1.06 except 1.00 are plotted in Figure 7, and the majority-spin, minority-spin and total gaps are shown in Figure 8. It is clearly seen that strained $\text{CrF}_{1.5}\text{I}_{1.5}$ monolayer are all indirect gap semiconductors in considered strain range. It is found that the majority-spin and total gaps coincide except 0.94 strain, which means that $\text{CrF}_{1.5}\text{I}_{1.5}$ monolayer holds half-semiconductor character. At 0.94 strain, the VBM is at minority-spin channel from previous majority-spin one. From 1.06 to 0.94 strain, strain makes both conduction and valence bands of minority-spin channel move toward Fermi level, which leads to the reduced minority-spin gap. The majority-spin gap shows a nonmonotonic behavior, which is mainly due to change of CBM. In fact, at 0.94 strain, the AF-Néel becomes ground state, and we plot the energy bands along with FM states in Figure 9 using orthorhombic supercell. The AF-Néel state still is an indirect gap semiconductor with the gap value of 1.282 eV , and the local magnetic moments of Cr is $2.893 \mu_B$.

The strain engineering has been proved to be an very effective way to enhance piezoelectric properties of 2D materials, and then the strain effects on piezoelectric properties of $\text{CrBr}_{1.5}\text{I}_{1.5}$ monolayer are performed. The elastic constants including C_{11} , C_{12} , $C_{11}-C_{12}$ and

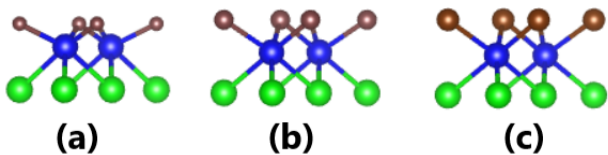


FIG. 14. (Color online) The side views of crystal structure of $\text{CrF}_{1.5}\text{I}_{1.5}$ (a), $\text{CrCl}_{1.5}\text{I}_{1.5}$ (b) and $\text{CrBr}_{1.5}\text{I}_{1.5}$ (c).

$C_{11}+C_{12}$ of $\text{CrBr}_{1.5}\text{I}_{1.5}$ monolayer with FM state as a function of biaxial strain are plotted in Figure 10, along with ones of AF-Néel state at 0.94 strain. It is clearly seen that C_{11} , C_{12} , $C_{11}-C_{12}$ and $C_{11}+C_{12}$ are all decreases with increasing strain from 0.94 to 1.06 strain. It is found that C_{11} , C_{12} , $C_{11}-C_{12}$ and $C_{11}+C_{12}$ with AF-Néel state are lower than ones with FM state at 0.94 strain. So, it is important to consider the magnetic configurations for calculating elastic constants. Calculated results show that the $\text{CrBr}_{1.5}\text{I}_{1.5}$ monolayer is mechanically stable in the considered strain range, since the calculated elastic constants satisfy the mechanical stability criteria⁴⁹.

The piezoelectric stress coefficients (e_{22} and e_{31}) along the ionic and electronic contributions and piezoelectric strain coefficients (d_{22} and d_{31}) of $\text{CrBr}_{1.5}\text{I}_{1.5}$ monolayer with FM state as a function of biaxial strain are plotted in Figure 11 and Figure 12, along with ones of AF-Néel state at 0.94 strain. It is found that the compressive strain can enhance the d_{22} due to improved e_{22} based on Equation 4, and the d_{22} improves to 0.993 pm/V at 0.94 strain from unstrained 0.557 pm/V. The tensile strain can decrease the d_{22} , and the d_{22} at 1.06 strain reduces to 0.039 pm/V due to very small e_{22} (0.0066×10^{-10} C/m). For d_{31} , the opposite strain dependence is observed, and the tensile strain can improve d_{31} due to reduced $C_{11}+C_{12}$. At 1.06 strain, the d_{31} of $\text{CrBr}_{1.5}\text{I}_{1.5}$ monolayer is 1.545 pm/V, increased by 36% with respect to unstrained one. In considered strain range, the electronic and ionic parts have opposite signs for both e_{22} and e_{31} , and they (absolute value) all decreases with strain from 0.94 to 1.06.

The magnetic configuration may have important effects on piezoelectric coefficients, and a magnetic phase transition may induce the jump of piezoelectric coefficients. We recalculate the e_{22} and e_{31} along the ionic and electronic contributions and d_{22} and d_{31} of $\text{CrBr}_{1.5}\text{I}_{1.5}$ monolayer with AF-Néel state at 0.94 strain. It is found that magnetic configuration has important effect on e_{22} from 0.285×10^{-10} C/m of FM state to 0.181×10^{-10} C/m of AF-Néel state, and has little influence on e_{31} (0.502×10^{-10} C/m for FM and 0.495×10^{-10} C/m for AF-Néel). The similar effects on d_{22} and d_{31} also can be found, and the d_{22} (d_{31}) changes from 0.993 pm/V (0.933 pm/V) of FM state to 0.677 pm/V (0.999 pm/V) of AF-Néel state. It is also found that magnetic configuration has important effects on both the electronic and ionic parts of e_{22} , and has neglectful influences on ones of e_{31} . So, it is very important to consider mag-

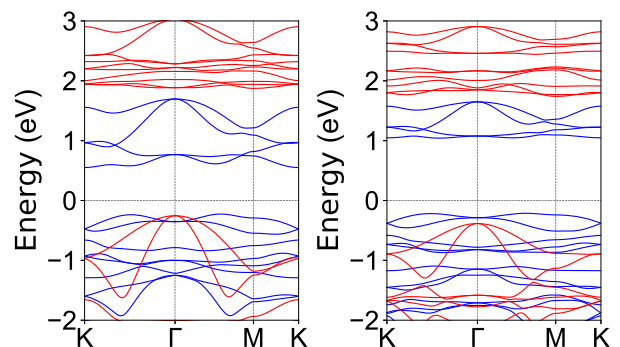


FIG. 15. (Color online) The energy band structures of $\text{CrF}_{1.5}\text{I}_{1.5}$ (Left) and $\text{CrCl}_{1.5}\text{I}_{1.5}$ (Right) with FM state. The blue (red) lines represent the band structure in the spin-up (spin-down) direction.

netic order for piezoelectric coefficients. It is interesting that the PAFM can be induced by compressive strain, which may open up potential opportunities for intriguing physics and novel devices.

VII. DISCUSSION AND CONCLUSION

In fact, one of two I layers of monolayer CrI_3 can also be replaced by F or Cl atoms, namely monolayer $\text{CrF}_{1.5}\text{I}_{1.5}$ and $\text{CrCl}_{1.5}\text{I}_{1.5}$. For $\text{CrCl}_{1.5}\text{I}_{1.5}$ monolayer, the FM order still is the ground state by comparing energy difference of four different initial magnetic configurations (Figure 2). However, for monolayer $\text{CrF}_{1.5}\text{I}_{1.5}$, the FM and AF-Néel orders have almost the same energy, and the difference is only 0.48 meV/ $\text{CrF}_{1.5}\text{I}_{1.5}$ formula. So, we focus on the FM state of both monolayer $\text{CrF}_{1.5}\text{I}_{1.5}$ and $\text{CrCl}_{1.5}\text{I}_{1.5}$ for a better comparison. For monolayer $\text{CrF}_{1.5}\text{I}_{1.5}$ ($\text{CrCl}_{1.5}\text{I}_{1.5}$), the optimized lattice constants is 6.250 (6.590) Å, and the calculated C_{11} and C_{12} are 49.97 (34.88) Nm^{-1} and 16.34 (9.94) Nm^{-1} , which satisfy the Born criteria of mechanical stability⁴⁹. From Figure 13, it is proved that monolayer $\text{CrF}_{1.5}\text{I}_{1.5}$ ($\text{CrCl}_{1.5}\text{I}_{1.5}$) is dynamically stable. The side views of crystal structures of $\text{CrX}_{1.5}\text{I}_{1.5}$ (X=F, Cl and Br) are plotted in Figure 14, and it is clearly seen that the distortions of octahedral environment located by Cr atoms become more and more severe with X from Br to Cl to F due to the more difference in atomic sizes and electronegativities of X and I atoms. It is found that an easy axis of monolayer $\text{CrCl}_{1.5}\text{I}_{1.5}$ is along the c-direction, and the corresponding MAE is 110 μeV per Cr atom. However, for monolayer $\text{CrF}_{1.5}\text{I}_{1.5}$, an easy axis is along the in-plane direction, and the MAE is up to 2151 μeV per Cr atom. Finally, the piezoelectric properties of monolayer $\text{CrF}_{1.5}\text{I}_{1.5}$ and $\text{CrCl}_{1.5}\text{I}_{1.5}$ are investigated, and their d_{31} is up to 2.578 pm/V and 1.804 pm/V, respectively. The related data are summarized in Table I. In fact, many PFMs can be achieved in 2D CrX_3 (X=F, Cl, Br and I) family by using the same design principle of mono-

layer $\text{CrBr}_{1.5}\text{I}_{1.5}$, for example Janus monolayer monolayer $\text{CrCl}_{1.5}\text{F}_{1.5}$, $\text{CrCl}_{1.5}\text{Br}_{1.5}$, $\text{CrBr}_{1.5}\text{F}_{1.5}$ and so on.

In summary, our theoretical calculations demonstrate that the PFM can occur in Janus $\text{CrBr}_{1.5}\text{I}_{1.5}$ monolayer with dynamic, mechanical and thermal stabilities, which possesses a sizable MAE. By breaking the inversion and mirror symmetry, both in-plane and out-of-plane piezoelectric polarizations can be induced by a uniaxial in-plane strain. Amazingly, the out-of-plane d_{31} (1.138 pm/V) is obviously higher compared with ones of many familiar 2D materials. It is proved that strain engineering can effectively tune piezoelectricity of monolayer $\text{CrBr}_{1.5}\text{I}_{1.5}$. The PAFM can also be realized by compressive strain, and d_{22} (d_{31}) is 0.677 pm/V (0.999 pm/V) at 0.94 strain. Finally, similar to $\text{CrBr}_{1.5}\text{I}_{1.5}$, the PFM can also be achieved in the monolayer $\text{CrF}_{1.5}\text{I}_{1.5}$

and $\text{CrCl}_{1.5}\text{I}_{1.5}$ with very large d_{31} being 2.578 pm/V and 1.804 pm/V. Our works supply an experimental proposal to achieve large out-of-plane piezoelectric response in PFMs, and hope that the work can stimulate further experimental effort on 2D PFM.

ACKNOWLEDGMENTS

This work is supported by Natural Science Basis Research Plan in Shaanxi Province of China (2021JM-456). We are grateful to the Advanced Analysis and Computation Center of China University of Mining and Technology (CUMT) for the award of CPU hours and WIEN2k/VASP software to accomplish this work.

-
- ¹ W. Wu, L. Wang, Y. Li, F. Zhang, L. Lin, S. Niu, D. Chenet, X. Zhang, Y. Hao, T. F. Heinz, J. Hone and Z. L. Wang, *Nature* **514**, 470 (2014).
 - ² H. Zhu, Y. Wang, J. Xiao, M. Liu, S. Xiong, Z. J. Wong, Z. Ye, Y. Ye, X. Yin and X. Zhang, *Nat. Nanotechnol.* **10**, 151 (2015).
 - ³ A. Y. Lu, H. Zhu, J. Xiao, C. P. Chuu, Y. Han, M. H. Chiu, C. C. Cheng, C. W. Yang, K. H. Wei, Y. Yang, Y. Wang, D. Sokaras, D. Nordlund, P. Yang, D. A. Muller, M. Y. Chou, X. Zhang and L. J. Li, *Nat. Nanotechnol.* **12**, 744 (2017).
 - ⁴ M. Dai, Z. Wang, F. Wang, Y. Qiu, J. Zhang, C. Y. Xu, T. Zhai, W. Cao, Y. Fu, D. Jia, Y. Zhou, and P. A. Hu, *Nano Lett.* **19**, 5416 (2019).
 - ⁵ L. Dong, J. Lou and V. B. Shenoy, *ACS Nano*, **11**, 8242 (2017).
 - ⁶ R. X. Fei, We. B. Li, J. Li and L. Yang, *Appl. Phys. Lett.* **107**, 173104 (2015).
 - ⁷ M. N. Blonsky, H. L. Zhuang, A. K. Singh and R. G. Hennig, *ACS Nano*, **9**, 9885 (2015).
 - ⁸ Y. Chen, J. Y. Liu, J. B. Yu, Y. G. Guo and Q. Sun, *Phys. Chem. Chem. Phys.* **21**, 1207 (2019).
 - ⁹ S. D. Guo, Y. T. Zhu, W. Q. Mu and W. C. Ren, *EPL* **132**, 57002 (2020).
 - ¹⁰ S. D. Guo, Y. T. Zhu, W. Q. Mu, L. Wang and X. Q. Chen, *Comp. Mater. Sci.* **188**, 110223 (2021)
 - ¹¹ Y. Guo, S. Zhou, Y. Z. Bai, and J. J. Zhao, *Appl. Phys. Lett.* **110**, 163102 (2017).
 - ¹² W. B. Li and J. Li, *Nano Res.* **8**, 3796 (2015).
 - ¹³ Dimple, N. Jena, A. Rawat, R. Ahammed, M. K. Mohanta and A. D. Sarkar, *J. Mater. Chem. A* **6**, 24885 (2018).
 - ¹⁴ S. D. Guo, X. S. Guo, Y. Y. Zhang and K. Luo, *J. Alloy. Compd.* **822**, 153577 (2020).
 - ¹⁵ N. Jena, Dimple, S. D. Behere and A. D. Sarkar, *J. Phys. Chem. C* **121**, 9181 (2017).
 - ¹⁶ J. H. Yang, A. P. Wang, S. Z. Zhang, J. Liu, Z. C. Zhong and L. Chen, *Phys. Chem. Chem. Phys.*, **21**, 132 (2019).
 - ¹⁷ S. D. Guo, W. Q. Mu, Y. T. Zhu and X. Q. Chen, *Phys. Chem. Chem. Phys.* **22**, 28359 (2020).
 - ¹⁸ S. D. Guo, W. Q. Mu, Y. T. Zhu, S. Q. Wang and G. Z. Wang, *J. Mater. Chem. C*, 2021, DOI: 10.1039/D1TC00414J.
 - ¹⁹ S. D. Guo, Y. T. Zhu, W. Q. Mu and X. Q. Chen, arXiv:2103.03456 (2021).
 - ²⁰ M. T. Ong and E.J. Reed, *ACS Nano* **6**, 1387 (2012).
 - ²¹ A. A. M. Noor, H. J. Kim and Y. H. Shin, *Phys. Chem. Chem. Phys.* **16**, 6575 (2014).
 - ²² J. Tan, Y. H. Wang, Z. T. Wang, X. J. He, Y. L. Liu, B. Wanga, M. I. Katsnelson and S. J. Yuan, *Nano Energy* **65**, 104058 (2019).
 - ²³ L. Dong, H. Kumar, B. Anasori, Y. Gogotsi and V. B. Shenoy, *J. Phys. Chem. Lett.* **8**, 422 (2017).
 - ²⁴ Y. Ma, Y. Dai, M. Guo, C. Niu, Y. Zhu and B. Huang, *ACS Nano*, **6**, 1695 (2012).
 - ²⁵ C. Gong, L. Li, Z. Li, H. Ji, A. Stern, Y. Xia, T. Cao, W. Bao, C. Wang, Y. Wang, Z. Q. Qiu, R. J. Cava, S. G. Louie, J. Xia and X. Zhang, *Nature* **546**, 265 (2017).
 - ²⁶ M. Khazaei, M. Arai, T. Sasaki, C. Y. Chung, N. S. Venkataramanan, M. Estili, Y. Sakka and Y. Kawazoe, *Adv. Funct. Mater.* **23**, 2185 (2013).
 - ²⁷ I. Choudhuri, S. Kumar, A. Mahata, K. S. Rawat and B. Pathak, *Nanoscale* **8**, 14117 (2016).
 - ²⁸ Y. Guo, H. Deng, X. Sun, X. Li, J. Zhao, J. Wu, W. Chu, S. Zhang, H. Pan, X. Zheng, X. Wu, C. Jin, C. Wu and Y. Xie, *Adv. Mater.* **29**, 1700715 (2017).
 - ²⁹ X. M. Wu, Y. L. Feng, S. Li, B. Q. Zhang and G. Y. Gao, *J. Phys. Chem. C* **124**, 16127 (2020).
 - ³⁰ B. Huang, G. Clark, E. Navarro-Moratalla, D. R. Klein, R. Cheng, K. L. Seyler, D. Zhong, E. Schmidgall, M. A. McGuire, D. H. Cobden, W. Yao, D. Xiao, P. Jarillo-Herrero and X. Xu, *Nature* **546**, 270 (2017).
 - ³¹ G. Bhattacharyya, I. Choudhuri, P. Bhauriyal, P. Garg and B. Pathak, *Nanoscale* **10**, 22280 (2018).
 - ³² W. B. Zhang, Q. Qu, P. Zhu and C. H. Lam, : *J. Mater. Chem. C* **3**, 12457 (2015).
 - ³³ S. Jiang, J. Shan and K. F. Mak, *Nat. Mater.* **17**, 406 (2018).
 - ³⁴ S. Jiang, L. Li, Z. Wang, K. F. Mak and J. Shan, *Nat. Nanotechnol.* **13**, 549 (2018).
 - ³⁵ N. Sivasdas, S. Okamoto, X. Xu, C. J. Fennie and D. Xiao, **18**, 7658 (2018).
 - ³⁶ Z. Wang, et al., *Nat. Commun.* **9**, 2516 (2018).
 - ³⁷ G. Z. Qin, H. M. Wang, L. C. Zhang, Z. Z. Qin and M. Hu, *J. Mater. Chem. C* **8**, 3520 (2020).

- ³⁸ B. Huang, et al., *Nat. Nanotechnol.* **13**, 544 (2018).
- ³⁹ A. Y. Lu, H. Y. Zhu, J. Xiao et al., *Nature Nanotechnology* **12**, 744 (2017).
- ⁴⁰ P. Hohenberg and W. Kohn, *Phys. Rev.* **136**, B864 (1964); W. Kohn and L. J. Sham, *Phys. Rev.* **140**, A1133 (1965).
- ⁴¹ G. Kresse, *J. Non-Cryst. Solids* **193**, 222 (1995).
- ⁴² G. Kresse and J. Furthmüller, *Comput. Mater. Sci.* **6**, **15** (1996).
- ⁴³ G. Kresse and D. Joubert, *Phys. Rev. B* **59**, 1758 (1999).
- ⁴⁴ J. P. Perdew, K. Burke and M. Ernzerhof, *Phys. Rev. Lett.* **77**, 3865 (1996).
- ⁴⁵ X. Wu, D. Vanderbilt and D. R. Hamann, *Phys. Rev. B* **72**, 035105 (2005).
- ⁴⁶ A. Togo, F. Oba, and I. Tanaka, *Phys. Rev. B* **78**, 134106 (2008).
- ⁴⁷ E. Mariani and F. V. Oppen, *Phys. Rev. Lett.* **100**, 076801 (2008).
- ⁴⁸ J. Carrete, W. Li, L. Lindsay, D. A. Broido, L. J. Gallego and N. Mingo, *Mater. Res. Lett.* **4**, 204 (2016).
- ⁴⁹ R. C. Andrew, R. E. Mapasha, A. M. Ukpong and N. Chetty, *Phys. Rev. B* **85**, 125428 (2012).
- ⁵⁰ A. A. M. Noor, H. J. Kim and Y. H. Shin, *Phys. Chem. Chem. Phys.* **16**, 6575 (2014).
- ⁵¹ M. T. Ong and E. J. Reed, *ACS Nano* **6**, 1387 (2012).
- ⁵² S. D. Guo, X. S. Guo, Z. Y. Liu and Y. N. Quan, *J. Appl. Phys.* **127**, 064302 (2020).
- ⁵³ L. Hu and X.R. Huang, *RSC Adv.* **7**, 55034 (2017).